ELSEVIER

Journal of Magnetism and Magnetic Materials 186 (1998) 199–213

Journal of magnetism and magnetic materials

Numerical calculation of the energy barrier distribution in disordered many-particle systems: the path integral method

D.V. Berkov*

INNOVENT e.V., Göschwitzer str. 22, D-07745, Jena, Germany

Received 22 September 1997; received in revised form 28 January 1998

Abstract

We present a numerical method for the evaluation of the distribution of energy barriers between metastable states in many-particle systems with arbitrary interparticle interaction. The method is based on the search for the optimal path between the two given metastable states using the minimization of the corresponding action occurring in the Onsager–Machlup functional for the transition probability between these two states. Test results for a non-interacting system of magnetic particles and for a dipolar magnetic glass are reported.

PACS: 02.70. − c; 05.20. − y; 75.10.N; 75.40.Mg; 75.50.Lk

Keywords: Many-particle systems; Numerical methods; Energy barrier distribution

1. Introduction

The problem of evaluating the transition probability between metastable states in various systems with many degrees of freedom is one of the most important and most difficult tasks in many areas of physics [1]. It is particularly important by studying disordered systems (e.g., random exchange spin glasses and dipolar glasses) with the strong interparticle interaction where disorder and frustration make not only analytical but also numerical calculations extremely difficult (see review articles [2–4] and references therein).

For energy barriers ΔE comparable with the temperature T direct Monte–Carlo simulations of the escape over the barrier using Langevin equation(s) for the system of interest are possible [1,5,6]. Unfortunately, this is no longer the case for the most interesting situation – high energy barriers (or in the low temperature limit $T \ll \Delta E$ – temperature much less than the typical energy barrier height) because the waiting time for the system escape from the local minima growth exponentially with the barrier height.

* Corresponding author. Fax: + 49 3641 282530; e-mail: dberkov@t-online.de.

0304-8853/98/$19.00
PII: S0304-8853(98)00078-X

On the other hand, for $T \ll \Delta E$ the task is somewhat simpler because in this limit it is sufficient to find the lowest saddle point (its height will give the corresponding energy barrier) between the two chosen minima on the energy landscape and then calculate the transition probability p using the Arrhenius–Van't Hoff formula ($p \sim \exp(-\Delta E/T)$).

Unfortunately, even the problem of finding such a saddle point cannot be solved analytically in a general case of a strongly interacting many-particle system. The reason is that such a point, being a point in the system coordinate space where all energy derivatives with respect to system coordinates $\partial E/\partial x_i$ are zero (but where neither a maximum nor a minimum of the system energy should be achieved!) can be found only as a solution of the corresponding system of equations $\partial E/\partial x_i = 0$, which are non-linear in a general case. We lack general methods for the solution of such systems, and there exist even arguments that there will never be any (see, e.g., Ref. [7]).

Reliable analytical and semi-analytical methods searching for saddle points in such systems are applicable only for a single [8,9] or few-particle case (for one of the latest attempts see Ref. [10]) so that the problem is still far from its final solution. In this paper we propose a method for the energy barrier evaluation based on the search for the optimal transition path between the two chosen metastable states by minimizing the corresponding action derived from the path-integral formulation of the problem. The required energy barrier can then be calculated as the barrier along this optimal trajectory. Further implementation depends on the task to be solved: if we are interested in the energy barrier distribution only, then it is sufficient to average over many such transitions between different pairs of metastable states; if we search for the transition between the two definite states (e.g., to study the magnetization relaxation from the metastable state with the relatively high energy to the state with the lowest energy) then we have to construct a connected path between these two states which goes maybe through some intermediate local minima and then compute the time dependence of the system magnetization using the transition sequence and the energy barriers found.

2. General idea

To explain the basic idea of our method we start with a system of N usual (i.e., not magnetic) classical particles which state can be described by cartesian coordinates x_i and corresponding velocities $\dot{x}_i$, $i = 1, \ldots, N$ (adjustments needed to apply the method to a system of magnetic moments will be explained in Section 4). If the interaction energy V of the particles depends on their coordinates only ($V = V\{\boldsymbol{x}\}$, where $\boldsymbol{x} = (x_1, \ldots, x_N)$) then the equations of motion for our system in the presence of thermal fluctuations (Langevin equations) can be written as

$$\dot{x}_i = -\frac{\partial V(\boldsymbol{x})}{\partial x_i} + \xi_i(t), \quad i = 1, \ldots, N, \tag{1}$$

where we have neglected the inertial term for the sake of simplicity (the whole method can be easily extended for the systems where this term is essential) and absorbed the friction constant into the time scaling. Random Langevin forces ξ_i which effect is assumed to simulate thermal fluctuations can be considered in most cases as independent random variables with the Gaussian distribution and zero correlation time [1] (for the ideas how one might generalize the method for the case of a colored noise, see, e.g., Refs. [11,12]):

$$\langle \xi_i(0)\xi_j(t)\rangle = 2D\delta_{ij}\delta(t), \tag{2}$$

where $D \sim T$.

For the assumptions made above the probability of some particular noise realization $\xi_i(t)$, $i = 1, \ldots, N$, for the time period $[0, t_f]$ is given by [13–15]

$$P[\boldsymbol{\xi}(t)] = A \exp\left[-\frac{1}{4D}\int_0^{t_f} \sum_i \xi_i^2 \, \mathrm{d}t \right]. \tag{3}$$

Rewriting the system (1) as $\xi_i(t) = \dot{x}_i + \partial V(\boldsymbol{x})/\partial x_i$ and introducing the Jacobian $J[\boldsymbol{x}(t)]$ of the variable transformation $\boldsymbol{x} \to \boldsymbol{\xi}$ we immediately obtain that the probability to observe a given trajectory $\boldsymbol{x}(t)$ for the transition between the two states A and B during the time t_f ($\boldsymbol{x}_A(0) \to \boldsymbol{x}_B(t_f)$) is [13,15,16]

$$P[\boldsymbol{x}(t)] = AJ[\boldsymbol{x}]\exp\left[-\frac{1}{4D}\int_0^{t_f} \mathrm{d}t \times \sum_i \left(\frac{\mathrm{d}x_i}{\mathrm{d}t} + \frac{\partial V(\boldsymbol{x})}{\partial x_i} \right)^2 \right]. \tag{4}$$

The total transition probability $(A \to B, t_f)$ is then given by the integral over all trajectories (paths) $\boldsymbol{x}(t)$:

$$P[A \to B, t_f] = A \int_{x_A}^{x_B} \boldsymbol{D}\boldsymbol{x}(t) J[\boldsymbol{x}] \times \exp\left[-\frac{S(\boldsymbol{x}(t), t_f)}{4D} \right], \quad (5)$$

where the *action* $S(\boldsymbol{x}(t))$ is defined as

$$S(\boldsymbol{x}(t), t_f) = \int_0^{t_f} dt \sum_i \left(\frac{dx_i}{dt} + \frac{\partial V(\boldsymbol{x})}{\partial x_i} \right)^2. \quad (6)$$

Evaluation of the path integral (5) in a general case is an immense task for any many-particle system where interparticle interaction cannot be treated using a simple perturbation theory. But for low- temperature limit it is obvious that the main contribution to Eq. (5) comes from the trajectories which are close to the optimal trajectory $\boldsymbol{x}_{opt}(t)$, i.e., to the trajectory which minimizes the action $S(\boldsymbol{x}(t))$. Hence, the energy barrier for the given transition can be found as the barrier along such a trajectory: $\Delta E(A \to B) = E_{max}(\boldsymbol{x}_{opt}) - E_A$. The problem we are left with is the minimization of the functional $S(\boldsymbol{x})$.

It is obviously impossible to perform this minimization analytically for any realistic model. There exist two main numerical possibilities: (i) write down the Euler–Lagrange equation for this functional and solve the corresponding boundary value problem or (ii) approximate the integral $S(\boldsymbol{x}(t))$ by some numerical quadrature formula and then minimize the function of many variables resulting from this approximation.

The first way leads to the system of N non-linear differential equations for functions $x_i(t)$, $i = 1, \ldots, N$, with the boundary conditions $x_i(0) = x_i^{(A)}$ and $x_i(t_f) = x_i^{(B)}$. The most powerful relaxation methods available for the solution of such systems require for each iteration the inversion of the system matrix which is full at least for the models with the long-range interaction; the case of 3D models with the short-range interaction leads to the band matrices with quite a large bandwidth ($\sim L^2$ for an $L \times L \times L$ system) which inversion is also very time-consuming [7].

For this reason we have chosen a direct minimization of the finite-difference version of Eq. (6). Dividing the time interval $[0, t_f]$ into K slices with the time step $\Delta t = t_f/K$ and approximating Eq. (6) by the simplest quadrature formula, we obtain

$$S_{disc(x)} = \Delta t \sum_{k=0}^{K-1} \sum_{i=1}^{N} \left[\frac{x_{i,k+1} - x_{i,k}}{\Delta t} + \frac{1}{2}\left(\frac{\partial V\{\boldsymbol{x}_{k+1}\}}{\partial x_{i,k+1}} + \frac{\partial V\{\boldsymbol{x}_k\}}{\partial x_{i,k}} \right) \right]^2, \quad (7)$$

where $x_{i,k}$ is the coordinate of the ith particle at the time $t_k = k\Delta t$, and $\boldsymbol{x}_k = (x_{i,k}, i = 1, \ldots, N)$ denotes the set of all particle coordinates for the kth slice. Thus, for a D-dimensional N-particle system we have to minimize a function of $D \cdot NK$ variables.

3. Algorithm details and results for the test system

The simplest possible test for the idea presented above is obviously the search of an optimal trajectory between the two minima for some simple energy landscape. To perform such a test, we have calculated the optimal trajectory for a particle moving in the 2D space (x_1, x_2) with the potential energy in the form

$$V(\boldsymbol{x}) = \sum_{j=1}^{J} \frac{U_j}{1 + \left(\frac{\boldsymbol{x} - \boldsymbol{r}_j}{\Delta_j} \right)^2}, \quad (8)$$

where $\boldsymbol{x} = (x_1, x_2)$ and $\boldsymbol{r} = (r_1, r_2)$ are vectors in the corresponding 2D space, the amplitudes are $U_j > 0$ (< 0) for the energy maxima (minima), parameter $\boldsymbol{r}_j$ determines the position and Δ_j the width of the jth peak (or hole), J is the total number of energy maxima and minima.

The result of such a test for the energy surface possessing 2 peaks (maxima) P_1 and P_2 and 2 holes (minima) M_1 and M_2 is shown in Fig. 1. The minimization of the action (7) for the potential (8) was performed using $K = 128$ time slices with $\Delta t = 0.25$. The starting trajectory was chosen as a straight line between the minima M_1 and M_2 and the final trajectory shown in Fig. 1 clearly passes through a saddle point providing the correct value of the energy barrier separating the two minima.

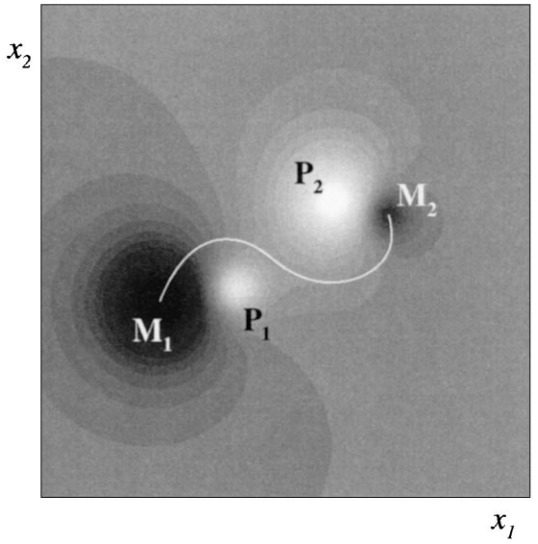

Fig. 1. Optimal trajectory (white line) for the particle transition between the two minima M_1 and M_2 for the potential of the type (8) found by the minimization of the corresponding action (7). On the grey scale map used to show the potential values bright zones correspond to the potential maxima.

For a many-particle systems of real interest with the particle number $N \gg 1$ the discrete action S_{disc} (7) (where the number of time slices K should also be large to ensure that the continuous action is approximated correctly by its finite-difference version) depends on the huge number of variables $\sim NK$; this alone makes its minimization very time-consuming. Additional difficulties usually occur due to the 'unpleasant' landscape of S_{disc} as a function of system coordinates – there are many long bend narrow valleys present. For this reason special care should be taken when choosing the minimization method (see Section 4). But although technically very difficult, the minimization of (7) itself is not the main problem when searching for the optimal trajectory between the two given metastable states. The main problem is the presence of many 'undesired' local minima of the functional (6), i.e., the presence of many trajectories between the states A and B in the system coordinate space which minimize Eq. (6) but do not provide any information about the corresponding energy barriers.

To present the simplest example where this problem appears, let us consider a 1D system of 2 *non-interacting* particles a and b which positions are given by the coordinates x_a and x_b with the potential energy $V(x_a, x_b) = V_a(x_a) + V_b(x_b)$ where each energy $V_{a(b)}$ has a double-well potential form, e.g.,

$$V_a(x_a) = \frac{U_{a1}}{1 + \left(\dfrac{x_a - r_{a1}}{\Delta_{a1}}\right)^2} + \frac{U_{a2}}{1 + \left(\dfrac{x_a - r_{a2}}{\Delta_{a2}}\right)^2}, \quad (9)$$

where the parameters $r_{a1(2)}$ define the positions, $\Delta_{a1(2)}$ the widths and $U_{a1(2)}$ (<0) the depths of the potential holes for the particle a; analogous potential is assumed to act on the particle b (in principle one might consider this example as a problem of the motion of a *single* particle in a 2D space (x_a, x_b) with a somewhat exotic potential $V = V_a(x_a) + V_b(x_b)$. The resulting 2D gray-scale plot of the energy surface is shown in Fig. 2; it is assumed that the potential minima (holes) are narrow enough so that they practically do not overlap. Minima are indicated as M_1–M_4 and saddle points as S_1–S_4. Potential energy values for each minimum and saddle points are also shown ($V(M_1) = -(U_{a1} + U_{b1})$, etc.). We would like to find the optimal path between the local minima M_1 and M_3 (Fig. 2).

The first fact we shall need to demonstrate the difficulty mentioned above is that for any path which minimizes the action (6) the conditions $\dot{x}_i = \pm\, \partial V\{\boldsymbol{x}\}/\partial x_i$ should be fulfilled; the plus (minus) sign corresponds to the 'downhill' ('uphill') trajectory parts. These conditions mean that the optimal trajectory goes along the gradient lines of the energy surface.

The second fact we need is that the value of the action $S(\boldsymbol{x})$ along the optimal path (trajectory) is proportional to the sum of the energy barriers which the path has to climb over: if the optimal trajectory consists of L pieces where the system moves 'uphill' and L pieces 'downhill' then the action value is

$$S(\boldsymbol{x}) = 4 \sum_{l=1}^{L} \Delta V_l, \quad (10)$$

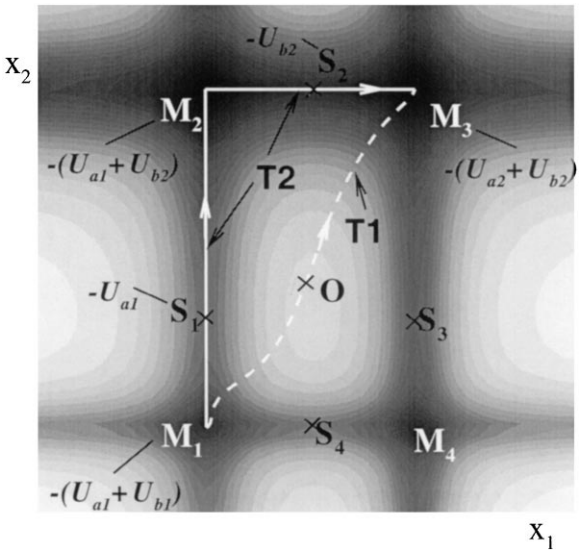

Fig. 2. Potential map for the system of two *non-interacting* particles each moving in a 1D double-well potential (9). Potential values for the minima M_1, M_2 and M_3 and the saddle points S_1 and S_2 are indicated in italic near the corresponding points. Trajectories T1 and T2 both minimize the action for the transition $M_1 \to M_3$ and the action values for both trajectories are equal (see text and Fig. 3 for details).

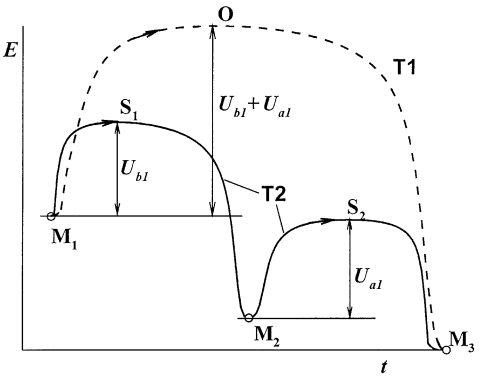

Fig. 3. Potential energies along the trajectories T1 and T2 shown in Fig. 2. The sums of the energy differences along the uphill parts of both trajectories are equal providing equal action values for T1 and T2.

where ΔV_l is the energy difference between the end and start points of the lth 'uphill' piece. Both these facts for a 1D case are proved, e.g., in Ref. [14]; the generalization to a multidimensional problem is straightforward.

According to these considerations, both paths $M_1 \to O \to M_3$(T1) and $M_1 \to S_1 \to M_2 \to S_2 \to M_3$(T2) shown in Fig. 2 deliver local extrema to the action for the transition $M_1 \to M_3$, because both paths are constructed to proceed along the gradient lines of the energy surface. It is also easy to show that both extrema in this situation are local minima of the action; in fact, both trajectories T1 and T2 were obtained by minimizing the action (7) with the potential (9) starting from different initial trajectories.

Moreover, from Eq. (10) it can be immediately seen that the *values* of $S[\boldsymbol{x}]$ for both trajectories are equal – see Fig. 3, where the system energy along the trajectories T1 and T2 is plotted. Namely, for the path T1 the energy increases from the starting point until the highest trajectory point O is reached and then decreases when the system moves downhill towards the final point M_3 (curve T1 in Fig. 3). The point O is far enough from all energy minima so that $V(O) = 0$. The energy difference along the uphill trajectory piece $M_1 \to O$ is $\Delta V_{T1} = V(O) - V(M_1) = U_{a1} + U_{b1}$. For the path T2 there are two uphill moves: from the starting point M_1 up to saddle S_1 (with the energy increase U_{b1}) and from the intermediate energy minimum M_2 up to saddle S_2 (energy increase U_{a1}), so that the total energy difference along the uphill trajectory pieces is $\Delta V_{T2} = U_{a1} + U_{b1}$, exactly as for the path T1.

Hence, both paths T1 and T2 are equivalent as long as we are interested in the *action value* only. However, it is clearly not the case, if we are going to gain information about the energy barriers which the system would encounter when jumping from the state M_1 to M_3: using the path T1 we would conclude that the smallest energy barrier the system has to overcome is $U_{a1} + U_{b1}$, whereby for this case it is evident that there exist a possibility to climb *subsequently* over two lower saddles S_1 and S_2 with the barriers U_{b1} and U_{a1} correspondingly (path T2).

The reason for this discrepancy is obvious (at least for the tutorial example shown): the trajectory T1 does not path through saddle points on the energy landscape, but rather through a local *maximum*. This means that to be able to extract the information about the energy barriers present in

our system from the 'optimal' trajectories we must be able to distinguish between 'optimal' trajectories passing (i) through energy saddle points and (ii) through local energy maxima.

One obvious possibility to discriminate between these two cases is the study of the curvature tensor of the energy surface along the given trajectory. However, this method is very time-consuming and subject to numerical instabilities due to the representation of the continuous trajectory as a discrete set of points (see Eq. (7)) and due to the finite accuracy by the determination of the 'optimal' trajectory. For this reason we have adopted another strategy: we jump a little bit aside from every trajectory point in a random direction and then try to minimize the system energy starting from this new position. If all energy minima found this way coincide with the minima which our trajectory has already 'seen' then we conclude that the trajectory indeed passes through saddle points. If some energy minimum does not coincide with those already observed along the trajectory then we state that the trajectory does not always pass through saddle points and do not use this trajectory when calculating energy barriers.

In the example considering above this algorithm would work as follows. Starting from any point lying a little bit apart from the trajectory T2 we would obviously land in the minima M_1, M_2 or M_3 which were already found along the path T2 so we would conclude that T2 really passes through the saddle points only. But when applying this method to the path T1 and jumping aside from, say, the point O, we would (after the subsequent energy minimization) finish very likely in one of the minima M_2 or M_4 which do not lie on the path under study (T1) thus leading to the conclusion that this trajectory does not (or at least not always) pass through saddle points.

The important question is how far apart from the trajectory points should we jump to the new points if we would like to reach another energy minimum after the energy minimization from this new points. The problem is that if we jump too far away then we might afterwards land in a new minimum even for a 'good' trajectory, e.g., when we jump from the point S_2 (Fig. 2) on the path T2 so far that we reach the point O, then minimizing from this point we can land in the minimum M_4 which would lead us to the wrong conclusion that T2 is a 'false' trajectory. On the other hand, if the jumps are too short, it can happen that we will not discover another minima even when starting from the points around the point O by testing the trajectory T1.

After trying several strategies we have confirmed, first of all, that the most important jumps are those performed from the points around the trajectory maxima (like the point O), as one would expect basing on the intuitive picture acquired from the images like shown in Fig. 1. For the jumps from such maxima the optimal jump length can be naturally defined using the values of the maximal energy gradient component in the vicinity of the maximum: we would like to jump so far that the maximal gradient component at the new point is M ($\gg 1$) times larger (see below) than the maximal gradient component at the maximum point (there is always a non-zero gradient at this point due to finite accuracy by the determination of the optimal trajectory). This guarantees us at least that the energy minimization starting from this new point will not terminate immediately claiming that this point is also an energy extremum. The concrete value of M depends on the problem under study; we have found that in most cases $M = 10$ is the adequate choice. When jumping from other points, we have usually chosen the jump length equal to the distance between the neighbouring trajectory points (recall that the jump direction is *random*).

Obviously, there exists also another kind of trajectories which minimize the action (6) and pass through the potential maxima. For example, for the potential surface shown in Fig. 1 the trajectory $M_1 \rightarrow M_2$ which would climb from the minimum M_1 to the peak P_1 along the gradient line and then go downhill to the minimum M_2 (again along the gradient line) would also provide a local minimum to the action functional (6). But for such a 'false' optimal trajectory the action *value* would be much larger than for the 'true' optimal path shown in Fig. 1 because the energy difference along the uphill part of this 'false' trajectory $\Delta V_f = V(P_1) - V(M_1)$ is larger than the corresponding value $\Delta V_t = V(S) - V(M_1)$ for the 'true' optimal path. Hence, some kind of a simulated

annealing algorithm can be applied to obtain quickly a rough approximation to the optimal trajectory which would be good enough as a starting point for a 'normal' minimization algorithm which would lead to the optimal trajectory with the lowest possible action value.

Next problem is the determination of the transition time t_f which is explicitly present in the continuous version of the action expression (6) and hence is required to set the time step and/or the number of time slices in the discrete version (7). Strictly speaking, for the rigorous determination of the transition time one should minimize the action also as a function of t_f; this process would lead to the action minimizations for several values of t_f chosen according, e.g., to the 'golden section search' procedure for the minimization of the single-variable function $S(t_f)$. However, due to the great effort required for one action minimization, such a method would be very time-consuming.

Fortunately, if we are interested in the energy barrier height only, we can use the fact that the value of this barrier depends on the transition time much weaker than the action value itself as it is illustrated in Table 1 for the energy barrier corresponding to the test potential (8) shown in Fig. 1. For this reason we have used the following method for the determination of t_f: we have minimized the action (7) with the (small) constant time step (usually $\Delta t = 0.25$–0.5) and various numbers of time slices K_l starting from some small number ($K_1 = 16$) and doubling it ($K_{l+1} = 2K_l$) for the next $(l+1)$th action minimization. The process was terminated for the given transition when the relative difference between the two values of the energy barriers obtained for the subsequent action minimizations was less than 1%: $|(E_l - E_{l+1})/E_l| < 0.01$. Usually the time slice numbers $K = 64$ or $K = 128$ were large enough to ensure this accuracy.

Energy landscapes for the two cases used to test this algorithm are shown in Fig. 4 (non-interacting 1D system of two particles with coordinates x_1 and x_2) and Fig. 5 (two interacting particles) where the gray-scale maps of the system energy $V(x_1, x_2)$ and transition trajectories between the potential minima found by our algorithm are shown. To find the optimal system trajectory between some two local (meta)stable states standard gradient methods were used for the discrete action minimization (7) starting from the straight trajectory between the two chosen minima.

Table 1
Dependencies of the energy barrier ΔE and action values S on the time slice number K used in the numerical approximation (7) of the action (6) for the transition $M_1 \rightarrow M_2$ shown in Fig. 1. The time step $\Delta t = 0.4$ is the same in all cases.

K	ΔE	S
32	3.2904	17.26
64	3.1724	14.58
128	3.1720	13.47
256	3.1720	13.12
512	3.1720	12.97

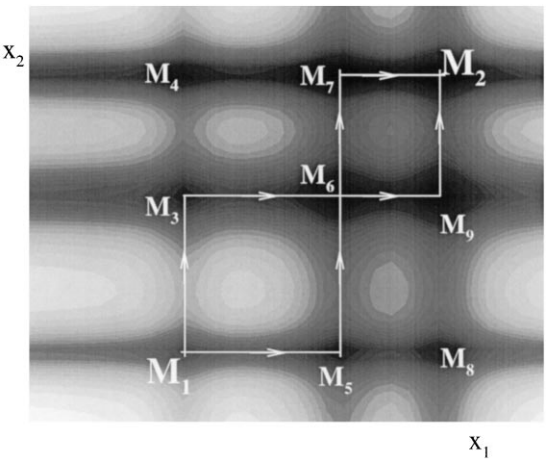

Fig. 4. Potential map for the system of two non-interacting particles each moving in the 1D three-well potential. Transitions between the local potential minima found by our algorithm when searching for the connected path between the minima M_1 and M_2 are shown.

Initially, the program was forced to start from the straight line $M_1 \rightarrow M_2$. After the 'optimal' trajectory for this transition was determined, the checking procedure described above was applied to this trajectory to find out whether it really passes through the saddle points only. In both examples shown in Figs. 4 and 5 it was not the case; in other words, some additional local energy minima were discovered during the check. Then the action minimization was performed for the trajectories

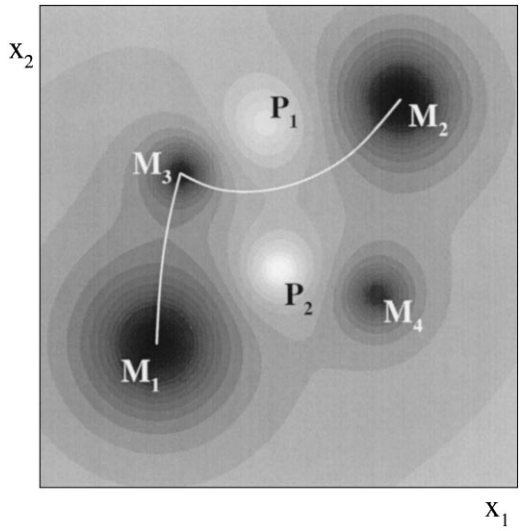

Fig. 5. The same as in Fig. 4 for two interacting particles.

between these new minima. To increase the probability of obtaining an optimal trajectory which passes through the saddle point only ('true' optimal trajectory), the transitions between the energy minima which were the nearest neighbours in the system coordinate space were studied first: for each local energy minima found during the previous checks the transitions between this minima and the fixed number p_{nn} of its nearest neighbours were analyzed. The search for the 'true' optimal trajectories was continued until the connected path between the initial M_1 and final M_2 states constructed from such trajectories was found.

Test result for the non-interacting case is presented in Fig. 4 where the potential used corresponds to the system of 2 non-interacting particles where each particle moves in a 3-well 1D potential like in Eq. (9). It can be seen that by searching for the transition path $M_1 \to M_2$ the algorithm has found out that this transition would occur via the intermediate states: it can be, e.g., the path $M_1 \to M_3 \to M_6 \to M_7 \to M_2$. Minima M_4 and M_8 were not discovered during the optimal trajectory searches for they are too far from the initial trajectory (straight line $M_1 \to M_2$) and the required connected path $M_1 \to M_2$ was found before the trajectories $M_3 \to M_7$ (which would enable to jump to M_4) and $M_5 \to M_9$ (possible jump to M_8) were analysed. The existence of more than one possible closed path between the initial and final states is due to the fact that the program does not stop immediately after the required path is discovered but investigates all transitions to the given number of nearest neighbours (in this case $p_{nn} = 2$) for each energy minima already found.

For the system of two interacting particles the algorithm was tested for a somewhat more complicated (when compared to Fig. 1) energy landscape of the type (8) shown in Fig. 5. Starting again from the straight line $M_1 \to M_2$ the algorithm was able to find the connected path $M_1 \to M_3 \to M_2$; the minimum M_4 was not accessible by jumping from the optimal trajectory obtained by minimizing the action for the direct transition $M_1 \to M_2$ and hence was not discovered during this search.

We have also performed various tests for more complicated energy surfaces than those shown in previous examples. All our tests led to qualitatively similar results: the algorithm described above did not succeed to find all minima of the system energy but was always able to find a connected trajectory between the two given local minima which passed through the saddle points only.

4. Implementation of the algorithm for magnetic particle systems

To apply the method presented above to the systems of interacting magnetic moments (classical exchange and dipolar spin glasses, systems of fine ferromagnetic particles, etc.) it is convenient to start with the equation of motion for the magnetic moment in the Landau–Lifshitz–Gilbert (LLG) form. Below we consider (for the definiteness) the system of small ferromagnetic particles, but the transfer of the method to the classical spin glass of any kind is obvious. The LLG-equation of motion for the particle magnetization $\boldsymbol{M}$ in the presence of thermal fluctuations can be written as (see [17] for detail)

$$\frac{d\boldsymbol{M}}{dt} = \gamma_0 \left[\boldsymbol{M} \times \left(\boldsymbol{H}^{\text{eff}} - \eta \frac{d\boldsymbol{M}}{dt} + \boldsymbol{H}^{\text{L}} \right) \right], \tag{11}$$

where γ_0 is the gyromagnetic ratio, η denotes the dissipation constant, the random (Langevin) field $\boldsymbol{H}^{\mathrm{L}}$ is assumed to simulate the effect of thermal fluctuations and the 'usual' effective field $\boldsymbol{H}^{\mathrm{eff}}$ is the negative derivative of the particle magnetic free energy density E over the magnetization

$$\boldsymbol{H}^{\mathrm{eff}} = -\frac{\partial E}{\partial \boldsymbol{M}}. \tag{12}$$

For the temperatures well below the Curie point of the particle material the magnitude of the magnetization vector remains constant and equal to the saturation magnetization M_{s}, so that the particle magnetization state is completely defined by the unit vector $\boldsymbol{m} = \boldsymbol{M}/M_{\mathrm{s}}$. The equation of motion for this vector is

$$\frac{\mathrm{d}\boldsymbol{m}}{\mathrm{d}t} = \gamma\left[\boldsymbol{m} \times \left(\boldsymbol{h}^{\mathrm{eff}} - \eta\frac{\mathrm{d}\boldsymbol{m}}{\mathrm{d}t} + \boldsymbol{h}^{\mathrm{L}}\right)\right], \tag{13}$$

where $\gamma = \gamma_0 M_{\mathrm{s}}$ and the reduced field $\boldsymbol{h} = \boldsymbol{H}/M_{\mathrm{s}}$ has been introduced. In the large dissipation limit $\eta\gamma \gg 1$ (which means the same as neglecting the inertial term in Eq. (1)) this equation can be rewritten in the form

$$\begin{aligned}\frac{\mathrm{d}\boldsymbol{m}}{\mathrm{d}t} &= -[\boldsymbol{m} \times [\boldsymbol{m} \times (\boldsymbol{h}^{\mathrm{eff}} + \boldsymbol{h}^{L})]\\ &= -\boldsymbol{m}(\boldsymbol{m}\boldsymbol{h}^{\mathrm{tot}}) + \boldsymbol{h}^{\mathrm{tot}},\end{aligned} \tag{14}$$

where all constants are absorbed in the time unit, the total field is $\boldsymbol{h}^{\mathrm{tot}} = \boldsymbol{h}^{\mathrm{eff}} + \boldsymbol{h}^{\mathrm{L}}$ and the normalization $\boldsymbol{m}^2 = 1$ was used by the last transformation.

The conservation of the magnetic moment magnitude makes the spherical coordinates (θ, ϕ) of the unit vector $\boldsymbol{m}$ to the 'natural' coordinates of our problem. Transforming all vectors to the new coordinate system with the z'-axis along the magnetic moment direction and the x'-axis lying in the meridian plane of the initial spherical coordinate system (so that in this initial system, as usual, $m_x = \sin\theta\cos\phi$, $m_y = \sin\theta\sin\phi$, $m_z = \cos\theta$), we obtain equations of motion for the magnetization angles

$$\dot{\theta} = -\frac{\partial E}{\partial \theta} + h^{\mathrm{L}}_{x'} \tag{15}$$

$$\sin\phi\cdot\dot{\phi} = -\frac{1}{\sin\theta}\frac{\partial E}{\partial \phi} + h^{\mathrm{L}}_{y'}, \tag{16}$$

where $h^{\mathrm{L}}_{x'}$ and $h^{\mathrm{L}}_{y'}$ are the Cartesian components of the Langevin field in the new coordinate system and the components of the 'usual' effective field are already expressed as the corresponding angular derivatives of the particle energy. It can be clearly seen from this equations that only those components of the Langevin field which are perpendicular to the magnetic moment direction are relevant for our consideration (exactly as only the perpendicular components of the 'usual' effective field are important for the description of the magnetic moment motion in the absence of thermal fluctuations).

The generalization to a system of N interacting particles is straightforward. In the resulting system of the equations of motion for the moment orientation angles (θ_i, ϕ_i)

$$\dot{\theta}_i = -\frac{\partial E\{\Omega\}}{\partial \theta_i} + h^{\mathrm{L}}_{i,\,x'} \tag{17}$$

$$\sin\phi_i\cdot\dot{\phi}_i = -\frac{1}{\sin\theta_i}\frac{\partial E\{\Omega\}}{\partial \phi_i} + h^{\mathrm{L}}_{i,y'}, \quad i = 1,\ldots,N, \tag{18}$$

the system energy $E\{\Omega\}$ (where Ω denotes the set of all angles (θ_i, ϕ_i)) includes now the interparticle interaction energy so that interaction of any kind (i.e., exchange, RKKY or dipolar) can be taken into account. This system is fully analogous to Eq. (1) so that under the same assumptions (that cartesian components of the Langevin field are independent random quantities with the Gaussian distribution) the transition probability between the two chosen magnetization states Ω_{A} and Ω_{B} can be expressed as

$$P[\Omega_{\mathrm{A}} \to \Omega_{\mathrm{B}}, t_{\mathrm{f}}] \simeq \int_{\Omega_{\mathrm{A}}}^{\Omega_{\mathrm{B}}} D\Omega(t) J[\Omega \to \boldsymbol{h}^{\mathrm{L}}] \times \exp\left[-\frac{S(\Omega(t), t_{\mathrm{f}})}{4D}\right], \tag{19}$$

where the action for the magnetic particle system is

$$S[\Omega(t)] = \int_0^{t_{\mathrm{f}}} \mathrm{d}t \sum_i \left[\left(\frac{\mathrm{d}\theta_i}{\mathrm{d}t} + \frac{\partial E\{\Omega\}}{\partial \theta_i}\right)^2 + \left(\sin\theta_i\frac{\mathrm{d}\phi_i}{\mathrm{d}t} + \frac{1}{\sin\theta_i}\frac{\partial E\{\Omega\}}{\partial \phi_i}\right)^2\right]. \tag{20}$$

The magnetization path in the Ω-space which minimizes this functional can provide information about the energy barrier separating the states Ω_A and Ω_B in the same way as for the test system discussed in Sections 2 and 3.

To find this optimal path, we have used the numerical quadrature representation of Eq. (20):

$$S_{\mathrm{disc}}(\boldsymbol{x}) = \Delta t \sum_{k=0}^{K-1} \sum_{i=1}^{N} \left[\frac{\theta_{i,k+1} - \theta_{i,k}}{\Delta t} + \frac{1}{2}\left(\frac{\partial E\{\Omega_{k+1}\}}{\partial \theta_{i,k+1}} + \frac{\partial E\{\Omega_k\}}{\partial \theta_{i,k}} \right) \right]^2 + \left[\frac{\sin\theta_{i,k+1} + \sin\theta_{i,k}}{2} \frac{\phi_{i,k+1} - \phi_{i,k}}{\Delta t} + \frac{1}{2}\left(\frac{1}{\sin\theta_{i,k+1}} \frac{\partial E\{\Omega_{k+1}\}}{\partial \phi_{i,k+1}} + \frac{1}{\sin\theta_{i,k}} \frac{\partial E\{\Omega_k\}}{\partial \phi_{i,k}} \right) \right]^2 \quad (21)$$

analogous to Eq. (7). Minimizing the corresponding discrete action S_{disc} as a function of orientation angles $(\theta_{i,k}, \phi_{i,k})$ of all particles for the time slices $k = 1, \ldots, K-1$ (moment coordinates for the 0th and Kth time slices are fixed being the given coordinates of the initial and final states) we were able to obtain the discrete representation of the optimal system trajectory. The same check procedure as described in Section 3 was applied to each trajectory found this way to ensure that it really passes through the saddle points. The energy barrier calculated along the 'true' optimal trajectory was assumed to be the lowest energy barrier between the two states Ω_A and Ω_B.

Apart from the usual difficulties encountered by the minimization of the many-variable functions, the minimization procedure for the discrete action (21) is subject to the stability problems specific for the spherical coordinates used. Namely, the factors $1/\sin\theta_i$ in (21) diverge for any trajectory closely approaching (at least at one slice) the polar axis of the spherical coordinate system ($\theta \to 0$ or $\theta \to \pi$). For this reason one has to choose suitable spherical coordinates for each particle separately at the beginning of the minimization procedure. Moreover, during the minimization process particle trajectories are moving in the angle space Ω so that the trajectory of some particle may become too close to the polar axis of its coordinate system even if at the beginning of the minimization it was not. Hence, one has also to watch for such 'dangerous' cases and switch to another spherical coordinate system for the corresponding particle when necessary.

The latter circumstance prevents, in particular, the usage of the most powerful standard minimization technique – the conjugate gradient method – because in this method the information about the previous minimization directions is stored during the minimization process. This information is partially lost when the coordinate system for any particle is changed which strongly decreases the performance of the conjugate gradients. The same problem occurs when spherical coordinates are used in the simulation of the quasistatic remagnetization processes in fine particle systems [18]. Switching to the Cartesian coordinates of the magnetic moments would not save the day, because these coordinates are *not* independent due to the conservation of the magnetic moment magnitude for each particle ($m_{x,i} + m_{y,i} + m_{z,i} = 1$) and the conjugate gradient method can be applied only in the case of independent coordinates (variables).

In principle, one can still try to modify the problem so that the conjugate gradient method could be applied. The two most obvious possibilities are: (i) introduction of the corresponding undetermined (Lagrange) multiplier for each moment to conserve its magnitude in Cartesian coordinates and (ii) usage of a penalty function which would strongly increase when the magnitude of any moment deviates from unity.

The first method has the disadvantage of increasing the number of independent variables (each Lagrange multiplier should be now considered as a new independent variable), so that in this case the number of variables would be $4N \cdot K$ instead of $2N \cdot K$ when using spherical coordinates.

By our attempts to apply the second method we have found that the corresponding minimization time was substantially larger even when compared with the simplest relaxation method with the adjustment of the relaxation step [19]. We propose the following explanation for this phenomenon. The major problem by the realization of this method is that the penalty function

should increase *fast* when the condition $|\boldsymbol{m}| = 1$ is violated to assure the conservation of the moment magnitude with the required high accuracy. This means that the curvature of the corresponding $3N \cdot K$-dimensional surface caused by this penalty function would be much larger than the curvature caused by the initial function (in our case – by the function which represents the discrete version of an action). This leads to the function landscape consisting of arbitrary bended tales with steep walls – surely the most unpleasant case for any minimization method including conjugate gradients.

For the reasons described above we have chosen for the minimization of Eq. (21) the improved version of the relaxation method derived from the 'equation of motion' method described in Refs. [18,19]. This improved version was developed by Hubert, Ramstöck and the author and is described in detail in Ref. [20]. We give here its brief description to make the paper self-contained.

The algorithm consists of three stages. At the first stage several 'relaxation steps' are made. The 'relaxation step' means moving the system coordinates in the direction of the local antigradient of the function f to be minimized:

$$x_i^{p+1} = x_i^p - \alpha_{\mathrm{rel}} \frac{\partial f(\boldsymbol{x}^p)}{\partial x_i} \tag{22}$$

with the step length α_{rel} chosen so that the function value decreases. If after some relaxation step the function value increases, we return to the previous point $\boldsymbol{x}^p$, decrease the step length $\alpha_{\mathrm{rel}} \to \alpha_{\mathrm{rel}}/2$ and perform the 'relaxation step' again until α_{rel} is small enough to ensure the decrease of f.

If during several (typically ~ 10) 'relaxation steps' with the constant α_{rel}-value the function decreased, we perform the full function minimization in the local antigradient direction, i.e., we perform the move (22) choosing the step length α so as to minimize the function value f (let us denote the corresponding length as α_f). Usually the step length α_f is *several hundred* times larger than α_{rel} which means that after several relaxation steps (22) with relatively small step length we are able to make a huge step in the desired direction.

The third stage is the minimization of the gradient norm along the local gradient direction starting from the new point where we have arrived after the full function minimization at the previous stage. This means that we perform the step (22) choosing α (which in principle can now be also negative) to minimize the sum

$$\|g\|^2 = \sum_i \left(\frac{\partial f(\boldsymbol{x}^p)}{\partial x_i} \right)^2 .$$

The purpose of this stage is to determine the step length for the subsequent normal 'relaxation steps' (stage one): α_{rel} for the next normal 'relaxation steps' is adjusted starting from the α-value obtained during this gradient norm minimization.

These three stages are repeated in the order described above until the convergence criterion (usually $|\partial f(\boldsymbol{x}^p)/\partial x_i| < \delta$ for all i) is satisfied.

Several comments are in order. First of all, for systems studied by us (micromagnetic simulations of domain walls [20], search of local minima for the Heisenberg spin glass [21], action minimization for the magnetic particle system described in this paper) this method provides the acceleration up to $\sim 10^3$ times when compared with the standard steepest descent algorithm [7] and unimproved 'equation of motion'-method [19] and is several times faster even in comparison with the preconditioned conjugate gradient method (NAG-library) when the latter can be applied.

Such an acceleration is obviously due to the large step length α_f during the second stage (the full function minimization). Although having no rigorous proof why should α_f always be so large, we would like to suggest an explanation why it is usually the case. To do this, we remind first of all that the standard steepest descent algorithm always tries to minimize the function in the antigradient direction (so that each step is the full minimization step in our notation). This often leads to the well known oscillations for the following reason: if the starting position is on one slope of the long and narrow valley, the local antigradient points to the valley floor (*not* to the function minimum and *not* along the valley) and moving in the antigradient direction up to the function minimum *along this direction* one usually finds himself on the opposite valley slope (and *not* on its floor, see, e.g., Refs. [7,22]). These jumps between the two slopes can

continue for quite a long time, moving very slowly towards the function minimum along the valley.

In our method we *do not minimize* the function along the antigradient direction during the relaxation steps on the first stage – we merely choose α_{rel} so that the function f decreases. This normally leads to the step length α_{rel} less than it would be for the full minimization along the antigradient direction. Hence, if we start from the point on the valley slope, after our 'relaxation step' we can land closer to the valley floor then after the full function minimization. After several such steps we can finish so close to the valley floor that the local antigradient at our location points almost *along* the valley (i.e., towards the function minimum) thus allowing us to do a huge step when performing the function minimization along the antigradient direction (the second stage).

The third stage is necessary to adjust the relaxation step α_{rel} because after performing the function minimization we can jump so far that the curvature of the valley where we are in may change substantially. We note that although the minimization of the gradient norm does not necessarily lead to the decrease of the function itself, it was almost always the case.

5. Test results for magnetic particle systems and discussion

To show the reliability of our algorithm for the saddle point search and the high performance of our function minimization method we have done calculations for several systems of magnetic particles.

For all systems studied below the particles are assumed to be absolutely single-domain (i.e., all spins within a single particle are collinear and the particle magnetic moment can only rotate as a whole). Further each particle is assumed to possess the uniaxial magnetic anisotropy of the easy-axis type, which means that its anisotropy energy can be written in the form $E_{an} = 0.5\beta M_s^2 V \sin^2\psi$ where V denotes the particle volume, β is the reduced anisotropy constant (for the easy axis case $\beta > 0$) and ψ denotes the angle between the easy axis direction $\boldsymbol{n}$ and the particle magnetic moment $\boldsymbol{m}$. Obviously, in the absence of the external field such a particle has two equivalent (meta)stable magnetization states along the two opposite directions of the anisotropy axis ($\psi = 0$ and $\psi = \pi$) separated by the reduced energy barrier $\varepsilon \equiv E/(M_s^2 V) = \beta/2$. The first test for our algorithm was performed on a single such particle and the energy barrier found agreed with the value listed above within the numerical accuracy.

In the second test the system of $N = 128$ *non-interacting* particles with different anisotropy constants β_i, $i = 1, \ldots, N$ was considered. In the absence of the external field such a system has 2^N metastable states (energy minima) with the same (zero) energy. Among them two states were chosen arbitrary and the algorithm had to find the connected path between these two states which passed through the saddle points only – the task analogous to the test example presented in Fig. 2, but now in the $2N$-dimensional space. From the physical point of view it is evident that transitions between the local minima of this system correspond to the single-particle moment jumps between the opposite directions of the anisotropy axis for the given particle. In all studied cases the algorithm indeed was able to find the connected path between the two chosen metastable states consisting of the single-moment flops. The energy barriers along this path for the jump of the moment of the ith particle agreed with the energy barrier evaluated as $\varepsilon_i = \beta_i/2$.

The last test was performed for a system of $N = 128$ *dipolarly interacting* particles with the single particle anisotropy. The particles were positioned randomly but non-overlapping in the cubic volume which size was chosen according to the prescribed particle volume concentration η (see below). For all particles the same anisotropy constant $\beta_0 = 2.0$ was taken. Thus the system energy in the absence of the external field can be written as

$$\frac{E}{M^2 V} = -\frac{\beta_0}{2}\sum_i (\boldsymbol{m}_i \boldsymbol{n}_i)^2 - \frac{1}{2}\sum_i \boldsymbol{m}_i \boldsymbol{h}_i^{dip}, \tag{23}$$

where the reduced dipole interaction field on the ith particle is (the factor $4\pi/3$ comes from the reduced distance units $r = R/a$, a being the particle radius)

$$\boldsymbol{h}_i^{dip} = \frac{4\pi}{3}\sum_{j\neq i} \frac{3\boldsymbol{e}_{ij}(\boldsymbol{e}_{ij}\boldsymbol{m}_j) - \boldsymbol{m}_j}{r_{ij}^3}. \tag{24}$$

The evaluation of the dipolar field (24) was performed using a Lorentz cavity method, i.e., only the field contributions from the particles which are at the distance $r < R_{\text{rest}}$ from the ith particle are evaluated via the sum (24). The contributions from the particles in the far zone are taken into account using the Lorentz field evaluated from the average system magnetization. The restriction radius R_{rest} was chosen so that its further increase did not change the interaction field obtained within the 1% accuracy limit; to achieve this accuracy, it was sufficient to take R_{rest} twice as large as the average interparticle distance for all concentrations studied. Periodic boundary conditions were assumed.

Using our algorithm we have evaluated the energy barrier distribution for various particle volume concentrations (Fig. 6). A large number of transitions between various pairs of the metastable states found for each case were analysed. Among them the following numbers of transitions which passed through the saddle points only were discovered and used to build histograms shown in Fig. 6: for $\eta = 0.001 - N_{\text{tr}} = 90$ transitions (180 barriers), for $\eta = 0.01 - N_{\text{tr}} = 194$ transitions (388 barriers), for $\eta = 0.08 - N_{\text{tr}} = 266$ transitions (532 barriers) and $\eta = 0.24 - N_{\text{tr}} = 159$ transitions (318 barriers). The whole calculation took about two weeks on the HP-Workstation 712/60 (60 MHz, 32 MB RAM, program code written in Fortran).

As expected, for the lowest concentration studied ($\eta = 0.001$, Fig. 6a) almost all barriers are nearly equal to the energy barrier $\varepsilon(\beta_0 = 2.0) = 1.0$ which corresponds to the single-moment jump, as it should be because in this case the interparticle interaction should have almost no influence.

Already for the next volume concentration $\eta = 0.01$ (Fig. 6b) there exists a considerable amount of barriers with another values, most of them being much lower than those corresponding to the single-moment jumps. They arise due to the quite strong interparticle interaction of particles which are by chance separated by a very small distance. In particular, the reduced interaction field from the nearest possible neighbour ($r_{ij} = 2a$, a being the particle diameter) is $h^{\text{dip}}_{\text{max}} \sim 1$ (see Eq. (24)) which is of the same order of magnitude as the maximal anisotropy field $h^{\text{an}}_{\text{max}} \sim \beta_0 = 2.0$ so that for the collective magnetic moment flop of such a pair of closely positioned particles any energy barrier can be expected.

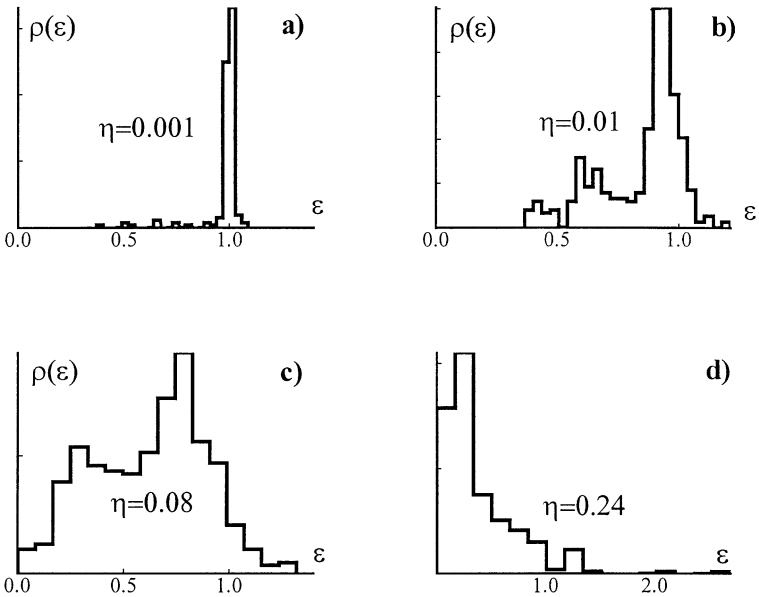

Fig. 6. Energy barrier distributions found by our algorithm for the system of $N = 128$ dipolarly interacting magnetic particles with the uniaxial anisotropy ($\beta = 2.0$) for various particle volume fractions as shown in the figure.

For the system with the moderate ($\eta = 0.08$, Fig. 6c) and high ($\eta = 0.24$, Fig. 6d) volume concentrations, the energy barrier distribution is qualitatively different from that observed for the low concentration case. It can be seen, that the distribution is shifted towards the lower energies, so that for the highest concentration studied the low energy barriers clearly dominate.

Although the results presented here for an interacting system are preliminary, we would like to make some comments concerning their comparison with experimental data (unfortunately there are to our knowledge no theoretical results which these distributions can be compared with). One might speculate that such a behaviour of energy barriers (shift of the distribution towards the lower energies with the increasing particle concentration) is consistent with the well known demagnetizing effect of the interparticle magnetodipolar interaction in fine particle systems below the blocking temperature (we recall that all our calculations are done in the low-temperature limit) – see papers in [23] and references therein. There are also some experimental evidences (see Refs. [24,25] for the latest examples) that the interparticle interaction leads to the faster magnetic relaxation which also means that the interaction shifts the energy barrier distribution towards the lower energies. Numerical MC simulations (based, however, on the single-particle updates) [26] seems to support this conclusion.

On the other hand, there exists a considerable amount of experimental results concerning the behaviour of the magnetic susceptability for, i.e., frozen ferrofluids (some recent results can be found in [27,28]), where it is demonstrated that the peak on the temperature dependence of the imaginary part of the AC susceptability $\chi''(T)$ [27] shifts towards larger temperatures with the increasing particle concentration. This means from the first glance that the interaction in such systems leads to higher energy barriers; but the relation between the energy barrier distribution and the susceptability in strongly interacting systems is by no means trivial. In particular, one has to take into account that by the transitions over the different barriers different moment changes occur and that such a transition itself may change the height of other barriers.

We would like also to point out that all these experiments – including those which seem to support our result – were performed at finite temperatures and on systems having a relatively broad distribution of the single-particle parameters (particle size, shape, anisotropy constant, etc.). Clearly further simulations and experiments are necessary.

6. Conclusions

We have developed and tested a numerical method which enables the evaluation of the energy barrier height for the transition between the two given metastable states of the many-particle system exploiting the minimization of the action for the corresponding transition. The method is suitable for the calculation of the energy barrier distribution in many-particle systems with continuous degrees of freedom and arbitrary interparticle interaction. In all test cases where the results could be compared with the known analytical values, our algorithm provided correct energy barrier heights. The major limitation of our algorithm in its present form is that it enables to evaluate the *energy* barriers only, whereby the *free energy* barriers are required to understand most properties of the many-particle systems for finite temperatures. The work concerning the corresponding expansion of the method is currently being performed.

References

[1] P. Hoenggi, P. Talkner, M. Borkovec, Rev. Mod. Phys. 62 (1990) 251.
[2] K. Binder, A.P. Young, Rev. Mod. Phys. 58 (1986) 801.
[3] V.S. Dotsenko, Sov. Physics – Usp. (USA) 36 (1993) 455.
[4] B.E. Vugmeister, M.D. Glinchuk, Rev. Mod. Phys. 62 (4) (1990) 993.
[5] J.M. Gonzalez, R. Ramirez, R. Smirnov-Rueda, J. Gonzalez, Phys. Rev. B 52 (1995) 16034.
[6] J.M. Sancho, A.M. Lacasta, M.C. Torrent, J. Garcia-Ojalvo, J. Tejada, Phys. Lett. A 181 (1993) 335.
[7] W.H. Press, S.A. Teukolsky, W.T. Vetterling, B.P. Flannery, Numerical Recipes in Fortran: the Art of Scientific Computing, Cambridge University Press, Cambridge 1992, p. 964.
[8] H.-B. Braun, J. Appl. Phys 76 (1994) 6310.
[9] I. Klik, L. Gunther, J. Appl. Phys. 67 (1990) 4505.
[10] A. Lyberatos, R.W. Chantrell, Phys. Rev. B 52 (1995) 4301.

[11] A.J. McKane, H.C. Luckock, A.J. Bray, Phys. Rev. A 41 (1990) 644.
[12] A.J. Bray, A.J. McKane, T.J. Newmann, Phys. Rev. A 41 (1990) 657.
[13] L. Onsager, S. Machlup, Phys. Rev. 91 (1953) 1505.
[14] A.J. Bray, A.J. McKane, Phys. Rev. Lett. 62 (1989) 493.
[15] R.P. Feynman, A.R. Hibbs, Quantum Mechanics and Path Integrals, McGraw-Hill, New York, 1965.
[16] R. Graham, Z. Phys. B 26 (1977) 281; R. Graham, in: T. Riste (Ed.), Fluctuations, Instabilities and Phase Transitions, Plenum, New York, 1975.
[17] W.F. Brown Jr., Phys. Rev. 130 (1963) 1677.
[18] D.V. Berkov, J. Magn. Magn. Mater 161 (1996) 337.
[19] D.V. Berkov, K. Ramstöck, A. Hubert, Phys. Stat. Sol (a) 137 (1993) 207.
[20] K. Ramstöck, Ph.D. Thesis, University Erlangen-Nürnberg, Germany, 1997.
[21] D.V. Berkov, to be published.
[22] F.S. Action, Numerical Methods that (usually) Work, The Math. Ass. of America Publ., Washington, DC, 1990.
[23] J.L. Dormann, D. Fiorani (eds.), Magnetic properties of Fine Particles, Proc. Int. Workshop in Rome, Italy, November 1991, North-Holland, Amsterdam, 1992.
[24] X. Battle, M. Garcia del Muro, A. Labarta, Phys. Rev. B 55 (1997) 6440.
[25] D. Fiorani et al., J. Magn. Magn. Mater 140–144 (1995) 395.
[26] R. Ribas, A. Labarta, J. Appl. Phys. 80 (1996) 5192.
[27] J. Zhang, C. Boyd, W. Luo, Ferrofluids, Phys. Rev. Lett. 77 (1996) 390.
[28] M. El-Hilo, K. O'Grady, J. Popplewell, R.W. Chantrell, N. Ayoub, J. de Phys. Coll. C8 48 (1988) 1835.